On the Performance of Optical Wireless Cooperative Systems over the DGG Fading Channel

Ehsan Soleimani-Nasab *, and Zabih Ghassemlooy †

*Department of Electrical and Computer Engineering, Graduate University of Advanced Technology, Kerman, Iran

†Optical Communications Research Group, Faculty of Engineering and Environment, Northumbria University, Newcastle, United Kingdom

Email: ehsan.soleimani@kgut.ac.ir, z.ghassemlooy@northumbria.ac.uk

Abstract: There is a growing research interests in hybrid optical and microwave wireless communications, which could be adpted in the next generation wireless networks. In this paper, based on the decode-and-forwardrelaying protocol and statistical behavior of the overall link's signal-to-noise-ratio, we consider six different practical scenarios by dering closed-form expressions for the outage and the bit error probabilities. Using Monte Carlo simulation we verify the predicted results. It is demonstrated that, decreasing the semi-angle of LED or increasing the filed of view of VLC receiver enhance the performance.

Keywords: Free space optical (FSO) communications, visible light communications (VLC), radio frequency (RF) communications, outage probability, bit error probability

1 Introduction

Recently, the lack of sufficient spectrum in radio frequency (RF)-based wireless systems

has shifted the focus to the complementary technology of optical wireless communications (OWC). OWC systems offer almost the same badwidth (i.e., data throughput) as the more established optical fiber communications (OFC), but with much reduced deployment cost and complexcity, since there are no need for cabeling, digging the roads, etc. [1]. In addition, OWC systems used in indoor and outdoor environments offer secure, safe and high data rates compared with RF wireles technologies [2]. In outdoor applications, OWC (mostly the free space optics and visible/infrared for the last mile and last meter access networks) can be used between base stations (BSs, BS and base station controllers (BSCs), BSC and mobile switching centers (MSCs) in the fifth generation (5G) cellular systems and beyond.

In certain application, the combination of RF, FSO and visible light communications (VLC) can be used in a cascaded (series) or parallel configurations to deliver high quality and high-speed connectivities between the transmiting and receiving end users. Such hybrid systems are adopted in the cooperative communications with two most widely used protocols, which are amplify-and-forward (AF) and decode-and-forward (DF) [3]. In [4], the performance of a hybrid RF-VLC relaying system considering Raician fadging channel was theoreticall investigated, and using Monte Carlo simulations, it was shown that there is a certain outage probability (OP) floor at higher signal to noise ratio (SNR) levels. The outage performance of a mixed RF/FSO-VLC system using a DF relay was analyzed in [5]. Assuming Gamma-Gamma turbulence channel and Rayleigh fading for the FSO and RF links, respectively the link with the maximum SNR is selected, with improved performance comparedg with FSO-VLC. In [6], theoretical investigation of the OP and biet error rate (BER) of a RF/VLC downlink employing a fixed gain AF relaying over Rayleigh fading channel was reported. Results showed outage probability improvement for transmission and reception angle of up to 45^{o}. In [7], a FSO-VLC DF relay link with cascaded dual-hop was reported by deriving close-form expressionse derived for OP and BER assuming a Gamma-Gamma turbulence channel, with validation of predicted results by means of Monte Carlo simulations. It was showed that, the link performance improved by increasing the semi-angle of the light emititing diode (LED) or the filed of view (FOV). A hybrid VLC-RF link using channel state information (CSI) with assisted AF and DF protocols was presented in [8], where the exact and asymptotic expressions for the OP and BER over Nakagami-m fading channel were derived. In [9], the performance of dual-hop mixed RF-FSO system with co-channel interference (CCI) was studied, where RF and FSO links were subjected to Nakagami-m fading and double

generalized Gamma (DGG) turbulence channels, respectively. The exact and asymptotical expressions for the OP and BER were derived and showed that, there are BER floor level for both cases of fixed gain and CSI-assisted relay schemes with constant average SNR values for the RF and FSO links, respectively. Finally, in [10] the performance of dual-hop mixed FSO-RF with the CSI-assisted AF, fixed gain AF and DF protocols was investigated by deriving expressions for the OP, BER and ergodic capacity over the extended generalized-K (EGK) and DGG fading channels. It was shown that, foe a fixed SNR for the RF link the diversity order of CSI-assisted protocol is equal to zero, i.e., no improvemment in the system performance.

In this work, we consider five practical scenarios of RF-FSO-VLC, FSO/RF-VLC, FSO-RF/VLC, RF/VLC-RF, VLC-RF-RF/VLC and FSO/RF-RF-RF/VLC systems and investigate their performance assuming DGG turbulence, Nakagami-m fading and circular uniform distribution for the FSO, RF and VLC links, respectively(s). Assuming both heterodyne detection (HD) and intensity modulation/direct detection (IM/DD) for the FSO link, we derive closed-form expressions for the OP and BER for each scenario in terms of Fox-H function. We show that, the RF/VLC-FSO offers the best performance among dual-hop systems, while RF-FSO has the worst performance. We also demonstrate that, RF-VLC-FSO has the best performance among triple-hop systems, while RF-FSO/RF-VLC display the worst performance.

The rest of the paper is organised as follow. In Section II, we introduce the system model and fading statistics under consideration. In Section III, we derive expressions for OP and BEP under the assumption of DF relaying. In Section IV, we present numerical results and finally conclude in Section V.

2 System Model and Fading Statistics

2.1 RF Link

The fading distribution of the RF link follows Nakagami-m model, with the probability density function (PDF) given by:

$$f_{\gamma_{\mathrm{RF}}}(\gamma) = \frac{\alpha^{m_{\mathrm{RF}}}\gamma^{m_{\mathrm{RF}}-1}}{\Gamma(m_{\mathrm{RF}})}e^{-\alpha\gamma} \tag{1}$$

where $\alpha = \frac{m_{\mathrm{RF}}}{\overline{\gamma}_{\mathrm{RF}}}$, $\overline{\gamma}_{\mathrm{RF}}$ is the average SNR per symbol and $\Gamma(m) = \int_0^\infty e^{-t}t^{m-1}\,dt$ is the Gamma function (GF) [11, Eq. (8.310.1)]. By utilizing [11, Eqs. (8.350.1, 8.350.2)] we can write

the cumulative distribution function (CDF) as [12, Eq. (9)]:

$$F_{\gamma_{\mathrm{RF}}}(\gamma) = \frac{\Upsilon(m_{\mathrm{RF}},\alpha\gamma)}{\Gamma(m_{\mathrm{RF}})} = 1 - \frac{\Gamma(m_{\mathrm{RF}},\alpha\gamma)}{\Gamma(m_{\mathrm{RF}})} \tag{2}$$

where $\Gamma(b,x) = \int_x^{\infty} e^{-t}t^{b-1}\,dt$ and $\Upsilon(b,x)$ are the upper and lower incomplete GFs, respectively [11, Eq. (8.350.2)]. Assuming, m_{RF} is an integer and utilizing [11, Eqs. (8.354.1, 8.352.4)], (2) can be rewritten as:

$$F_{\gamma_{\mathrm{RF}}}(\gamma) = 1 - \exp(-\alpha\gamma)\sum_{i=0}^{m_{\mathrm{RF}}-1}\frac{1}{i!}(\alpha\gamma)^i \tag{3}$$

The RF receiver (RF) selects the link with the maximum instantaneous SNR (i.e., $\Gamma_{\mathrm{RF}}^{\max} = \max\left(\Gamma_{\mathrm{RF}_k}\right)$ for $k = 1,\ldots,K$. The CDF of $\Gamma_{\mathrm{RF}}^{\max}$ is then written as:

$$F_{\Gamma_{\mathrm{RF}}^{\max}}(\gamma) = \prod_{k=1}^{K} F_{\Gamma_{\mathrm{RF}_k}}(\gamma) \tag{4}$$

2.2 FSO Link

FSO links are subject to the independent and non-identically distributed (i.n.i.d.) DGG fading distribution with pointing error impairments. γ denotes the instantaneous SNR with the PDF and CDF, respectively specified in [10, Eqs. (19, 20)], which is given as:

$$f_{\gamma_{\mathrm{FSO}}}(\gamma) = \frac{A_3 v}{\gamma} H_{r,u}^{u,0}\left[\frac{C^{1/v}\gamma}{\mu}\middle|\begin{matrix}(\kappa_3; v^{-1}1_r)\\(\kappa_4; v^{-1}1_u)\end{matrix}\right] \tag{5}$$

$$F_{\gamma_{\mathrm{FSO}}}(\gamma) = 1 - A_3 H_{r+1,u+1}^{u+1,0}\left[\frac{C^{1/v}\gamma}{\mu}\middle|\begin{matrix}[1,\kappa_3];[1,v^{-1}1_r]\\[0,\kappa_4];[1,v^{-1}1_u]\end{matrix}\right] \tag{6}$$

where $H_{p,q}^{m,n}[.]$ is Fox-H function defined in [13, Eq. (1.2)], $A_3 = \frac{\xi^2\sigma^{\beta_1-\frac{1}{2}}\lambda^{\beta_2-\frac{1}{2}}(2\pi)^{1-\frac{r(\lambda+\sigma)}{2}}r^{\beta_1+\beta_2-2}}{\alpha_2\lambda\Gamma(\beta_1)\Gamma(\beta_2)}$, $\xi = \frac{w_e}{2\sigma_s}$ is the ratio between the equivalent beam width at the Rx and the pointing error displacement standard deviation (i.e., jitter), and μ_i is the average electrical SNR of the ith FSO link. Here, α_1, α_2, β_1, β_2, Ω_1 and Ω_2 are identified using the variance of the small and large scale fluctuations of the laser beam [14]. λ and σ are positive integers such that $\frac{\lambda}{\sigma} = \frac{\alpha_1}{\alpha_2}$.

Other parameters are defined as $u = r(1+\lambda+\sigma)$, $v = \alpha_2\lambda$, $C = \left(\frac{A_2h^v}{r(\lambda+\sigma)}\right)^r$, $h = \frac{A_1B_1}{(1+\xi^2)A_2^{1/v}}$, $A_1 = \frac{\xi^2\sigma^{\beta_1-\frac{1}{2}}\lambda^{\beta_2-\frac{1}{2}}(2\pi)^{1-\frac{(\lambda+\sigma)}{2}}}{\Gamma(\beta_1)\Gamma(\beta_2)}$, $A_2 = \frac{\beta_1^{\sigma}\beta_2^{\lambda}}{\lambda^{\lambda}\sigma^{\sigma}\Omega_1^{\sigma}\Omega_2^{\lambda}}$, $B_1 = \prod_{j=1}^{\sigma+\lambda}\Gamma\left(\frac{1}{v}+\kappa_{1,j}\right)$, where $\kappa_{1,j}$ is the jth-

term of κ_1. $\kappa_1 = [\Delta(\sigma:\beta_1), \Delta(\lambda:\beta_2)]$, $\kappa_3 = \left[\Delta(r:\frac{\xi^2+v}{v})\right]$ comprising of r-term, and $\kappa_4 = [\Delta(r:\kappa_2)]$ comprising of u-term such that $\kappa_2 = \left[\frac{\xi^2}{v}, \kappa_1\right]$, $[\Delta(z:a_m)] \triangleq \Delta(z:a_1), \Delta(z:a_2)\ldots, \Delta(z:a_m)$ and $\Delta(j:x) \triangleq x/j, \ldots, (x+j-1)/j$. r is the detection type parameter (i.e., r = 1 and 2 represents HD and IM/DD schemes, respectively), and $1_n = [1,1,\ldots,1]$ comprising of n-term. The FSO Rx selects the link with $\Gamma_{\text{FSO}}^{\max} = \max\left(\Gamma_{\text{FSO}_j}\right)$ for $j = 1, \ldots, M$. The CDF of $\Gamma_{\text{FSO}}^{\max}$ is then written as:

$$F_{\Gamma_{\text{FSO}}^{\max}}(\gamma) = \prod_{j=1}^{M} F_{\Gamma_{\text{FSO}_j}}(\gamma) \tag{7}$$

2.3 VLC Link

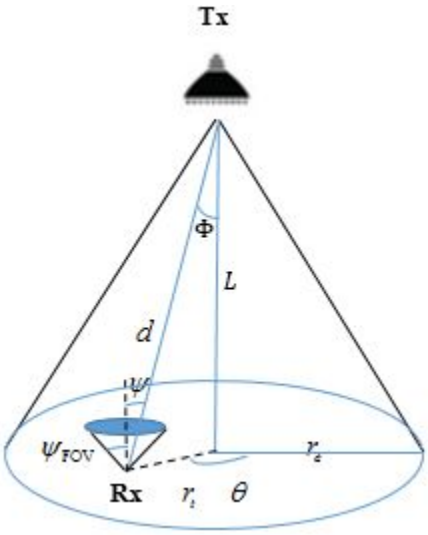

Fig. 1: A VLC system model

A tyrpical VLC link is shown in Fig. 1, which comprises of a LED-based transmitter (Tx) lamp placed at the ceiling at the height of L from a single mobile end user terminal (i.e., photodetector-based Rx).The Tx is modeled using a generalized Lambertian emission pattern with the order $m = -\frac{\ln 2}{\ln\cos\left(\phi_{\frac{1}{2}}\right)}$., where $\phi_{1/2}$ is the semi-angle at the half power of LED. Note, The maximum radius of a LED cell footprint $r_e = L\tan\left(\phi_{1/2}\right)$. Furthermore, the photodetector Rx is

characterized by its physical surface area A, responsivity R_p, gain of the optical filter U and the optical concentrator $g(\psi) = \frac{\rho^2}{\sin^2(\psi_{\mathrm{FOV}})} \prod \left(\frac{\psi}{\psi_{\mathrm{FOV}}}\right)$, where ρ is the refractive index of the lens at the Rx and ψ_{FOV} is the FOV of the Rx. Based on aforementioned definitions, the DC channel gain of the line of sight path between the Tx and the Rx in terms of the distance d and the angle $\theta$is given by [2]:

$$h_{\mathrm{VLC}} = \frac{A(m+1)R_p}{2\pi d^2} \cos^m(\varphi) U g(\psi) \cos(\psi) \prod \left(\frac{\psi}{\psi_{FOV}}\right) \tag{8}$$

where $\prod (x) \begin{cases} 1 & \mathrm{if} \quad x \le 1 \\ 0 & \mathrm{if} \quad x > 1. \end{cases}$

.From Fig. 1, we have $\cos(\psi) = \cos(\varphi) = L/d$, where $d = (r_t^2 + L^2)^{\frac{1}{2}}$. Therefore, the channel gain can be re-written as:

$$h_{VLC} = \frac{\Xi(m+1)L^{m+1}}{(r_t^2+L^2)^{\frac{m+3}{2}}} \tag{9}$$

where

$$\Xi = \frac{1}{2\pi} A R_p U g(\psi) \tag{10}$$

Each user is randomly located in a circle with a uniform distribution with the PDF given as:

$$f_{r_t}(r) = \frac{2r}{r_e^2} \quad 0 \le r \le r_e \tag{11}$$

Employing (9) and (10) and using the theory of random variables (RVs), the PDF of h_{VLC} is obtained as:

$$f_{h_{\mathrm{VLC}}}(h) = \frac{2}{r_e^2(m+3)} (\Xi(m+1)L^{m+1})^{\frac{2}{m+3}} h^{-\frac{2}{m+3}-1} \tag{12}$$

For a single VLC link with the instantaneous SNR $\Gamma_{\mathrm{VLC}} = \overline{\gamma}_{\mathrm{VLC}} \ h_{\mathrm{VLC}}^2$, the PDF is given by:

$$f_{\Gamma_{\mathrm{VLC}}}(\gamma) = \frac{\overline{\gamma}_{VLC}^{\frac{1}{m+3}}}{r_e^2(m+3)} (\Xi(m+1)L^{m+1})^{\frac{2}{m+3}} \gamma^{-\frac{m+4}{m+3}} \tag{13}$$

where $\overline{\gamma}_{\mathrm{VLC}} = \frac{\rho^2 P_{opt}^2}{N_0 B}$, $\gamma \in [\lambda_{\min}, \ \lambda_{\max}]$, $\lambda_{\min} = \frac{\overline{\gamma}_{\mathrm{VLC}}(\Xi(m+1)L^{m+1})^2}{(r_e^2+L^2)^{m+3}}$ and $\lambda_{\max} = \frac{\overline{\gamma}_{\mathrm{VLC}}(\Xi(m+1)L^{m+1})^2}{L^{2(m+3)}}$. Here P_{opt} represents the LED's average transmit optical power, N_0 is noise spectral density and B is baseband modulation bandwidth. Then, the CDF of the instantaneous SNR of ith VLC link for $\lambda_{\min} \le \gamma \le \lambda_{\max}$ is derived by:

$$F_{\Gamma_{\mathrm{VLC}_i}}(\gamma) = 1 + \frac{L^2}{r_e^2} - \frac{1}{r_e^2} (\Xi(m+1)L^{m+1})^{\frac{2}{m+3}} \left(\frac{\gamma}{\overline{\gamma}_{\mathrm{VLC}}}\right)^{\frac{-1}{m+3}} \tag{14}$$

For $\gamma \geq \lambda_{\max}$, $F_{\Gamma_{\mathrm{VLC}_i}}(\gamma) = 1$. The VLC Rx selects the link with $\Gamma_{\mathrm{VLC}}^{\max} = \max(\Gamma_{\mathrm{VLC}_i})$ for $i = 1, \ldots, N$. The CDF of $\Gamma_{\mathrm{VLC}}^{\max}$ is:

$$F_{\Gamma_{VLC}^{\max}}(\gamma) = \prod_{i=1}^{N} F_{\Gamma_{\mathrm{VLC}_i}}(\gamma) \tag{15}$$

3 Performance Analysis

For analyzing the performance of end-to-end system, we define performance assessment metric of OP, which defines the SNR of the end-to-end system falling bellow a predetermined SNR (i.e., threshold SNR), and is given as:

$$P_{out}(\gamma_{th}) = \Pr(\Gamma_{e2e} < \gamma_{th}) = F_{\Gamma_{e2e}}(\gamma_{th}) \tag{16}$$

We consider five scenarios with different combinations of the RF, FSO and VLC as shown in Fig. 1.

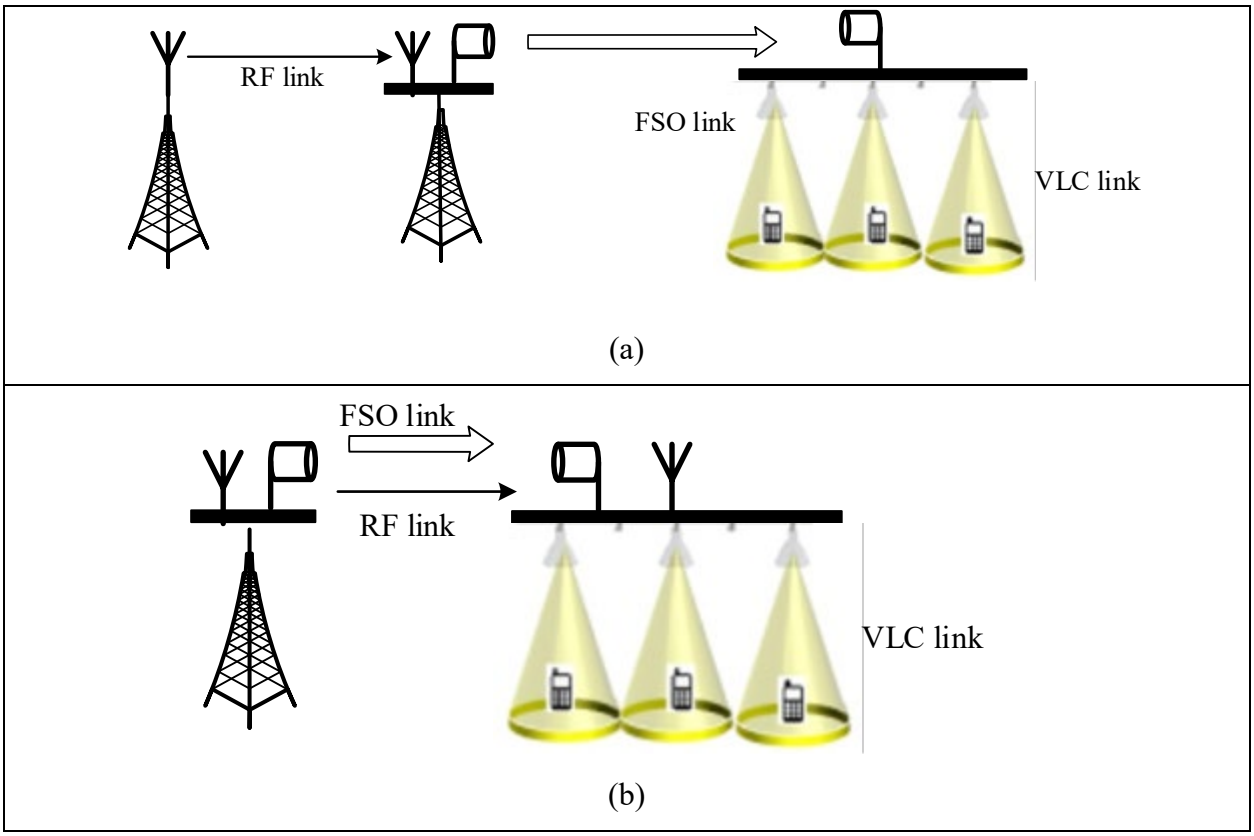

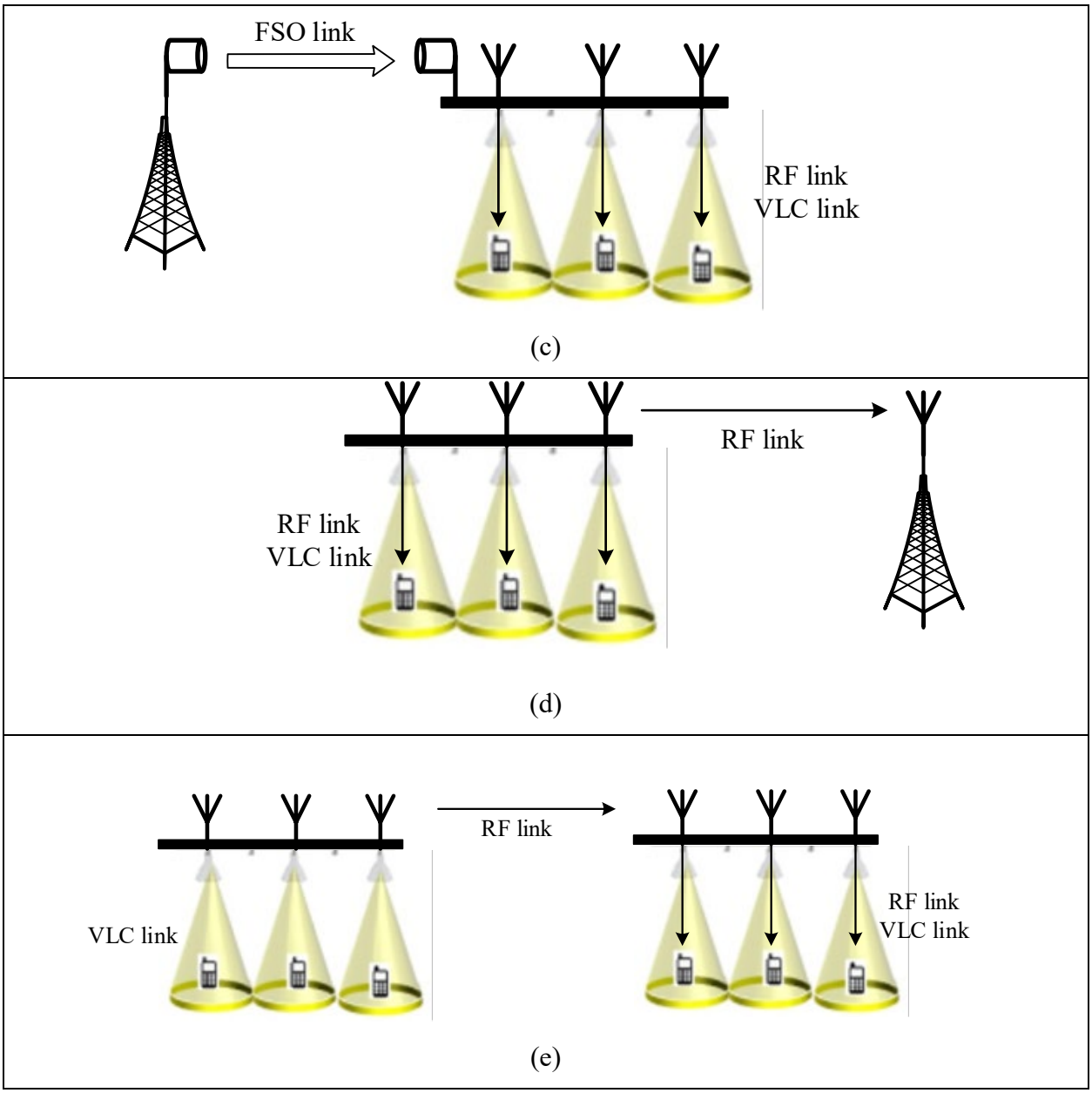

Figure 1: The system model for Scenarios: (a) I, RF-FSO-VLC, (b) II, RF/FSO-VLC, (C) III, FSO-RF/VLC, (d) IV, RF/VLC-RF, and (e) V, VLC-RF-RF/VLC

The end-to-end SNR for Scenarios I to V, respectively are given as:

$$\Gamma_{e2e}^{I} = \min(\Gamma_{VLC}^{\max}, \Gamma_{\mathrm{FSO}}, \Gamma_{\mathrm{RF}}) \tag{17a}$$

$$\Gamma_{e2e}^{II} = \min(\max(\Gamma_{\mathrm{FSO}}, \Gamma_{\mathrm{RF}}), \Gamma_{\mathrm{VLC}}^{\max}) \tag{17b}$$

$$\Gamma_{e2e}^{III} = \min(\Gamma_{FSO}, \max(\Gamma_{RF}^{\max}, \Gamma_{VLC}^{\max})) \tag{17c}$$

$$\Gamma_{e2e}^{IV} = \min(\max(\Gamma_{RF_1}^{\max}, \Gamma_{VLC}^{\max}), \Gamma_{RF_2}) \tag{17d}$$

$$\Gamma_{e2e}^{V} = \min(\Gamma_{VLC_1}^{\max}, \Gamma_{\mathrm{R}F_1}, \max(\Gamma_{\mathrm{R}F_2}^{\max}, \Gamma_{VLC_2}^{\max})) \quad (17e)$$

Using the RV theory the end-to-end CDFs for Scenarios I to V, respectively are given as:

$$F_{\Gamma_{e2e}}^{I}(\gamma) = F_{\Gamma_{\mathrm{FSO}}}(\gamma) + F_{\Gamma_{\mathrm{RF}}}(\gamma) + F_{\Gamma_{\mathrm{VLC}}^{\max}}(\gamma)$$
$$-F_{\Gamma_{\mathrm{FSO}}}(\gamma)F_{\Gamma_{\mathrm{RF}}}(\gamma) - F_{\Gamma_{FSO}}(\gamma)F_{\Gamma_{\mathrm{VLC}}^{\max}}(\gamma)$$
$$-F_{\Gamma_{\mathrm{RF}}}(\gamma)F_{\Gamma_{\mathrm{VLC}}^{\max}}(\gamma) + F_{\Gamma_{\mathrm{FSO}}}(\gamma)F_{\Gamma_{\mathrm{RF}}}(\gamma)F_{\Gamma_{VLC}^{\max}}(\gamma) \quad (18a)$$

$$F_{\Gamma_{e2e}}^{II}(\gamma) = F_{\Gamma_{FSO}}(\gamma)F_{\Gamma_{\mathrm{R}F}}(\gamma) + F_{\Gamma_{VLC}^{\max}}(\gamma)$$
$$-F_{\Gamma_{\mathrm{FSO}}}(\gamma)F_{\Gamma_{\mathrm{R}F}}(\gamma)F_{\Gamma_{VLC}^{\max}}(\gamma) \quad (18b)$$

$$F_{\Gamma_{e2e}}^{III}(\gamma) = F_{\Gamma_{\mathrm{FSO}}}(\gamma) + F_{\Gamma_{FSO}}(\gamma)F_{\Gamma_{\mathrm{VLC}}^{\max}}(\gamma)$$
$$-F_{\Gamma_{FSO}}(\gamma)F_{\Gamma_{\mathrm{R}F}^{\max}}(\gamma)F_{\Gamma_{VLC}^{\max}}(\gamma) \quad (18c)$$

$$F_{\Gamma_{e2e}}^{IV}(\gamma) = F_{\Gamma_{\mathrm{R}F_1}^{\max}}(\gamma)F_{\Gamma_{VLC}^{\max}}(\gamma) + F_{\Gamma_{\mathrm{R}F_2}}(\gamma)$$
$$-F_{\Gamma_{\mathrm{R}F_1}^{\max}}(\gamma)F_{\Gamma_{\mathrm{R}F_2}}(\gamma)F_{\Gamma_{VLC}^{\max}}(\gamma) \quad (18d)$$

$$F_{\Gamma_{e2e}}^{V}(\gamma) = F_{\Gamma_{\mathrm{VLC}_1}^{\max}}(\gamma) + F_{\Gamma_{\mathrm{R}F_1}}(\gamma) + F_{\Gamma_{VLC_2}^{\max}}(\gamma)F_{\Gamma_{\mathrm{R}F_2}^{\max}}(\gamma)$$
$$-F_{\Gamma_{\mathrm{VLC}_1}^{\max}}(\gamma)F_{\Gamma_{\mathrm{R}F_1}}(\gamma) - F_{\Gamma_{VLC_2}^{\max}}(\gamma)F_{\Gamma_{\mathrm{R}F_1}}(\gamma)F_{\Gamma_{\mathrm{R}F_2}^{\max}}(\gamma)$$
$$-F_{\Gamma_{\mathrm{VLC}_1}^{\max}}(\gamma)F_{\Gamma_{\mathrm{R}F_2}^{\max}}(\gamma)F_{\Gamma_{VLC_2}^{\max}}(\gamma)$$
$$+F_{\Gamma_{\mathrm{VLC}_1}^{\max}}(\gamma)F_{\Gamma_{\mathrm{R}F_2}^{\max}}(\gamma)F_{\Gamma_{VLC_2}^{\max}}(\gamma)F_{\Gamma_{\mathrm{R}F_1}}(\gamma) \quad (18e)$$

4 Monte Carlo Simulation

In this section, we validate the analysis carried out by means of the OP performance for the following turbulence parameters (i) DGG strong: $\alpha_1 = 1.8621, \alpha_2 = 1, \beta_1 = 0.5, \beta_2 = 1.8, \Omega_1 = 1.5074, \Omega_2 = 0.928$; (ii) DGG moderate: $\alpha_1 = 2.169, \alpha_2 = 1, \beta_1 = 0.55, \beta_2 = 2.35, \Omega_1 = 1.5793, \Omega_2 = 0.9671$; (iii) DGG weak: $\alpha_1 = 2.1, \alpha_2 = 2.1, \beta_1 = 4, \beta_2 = 4.5, \Omega_1 = 1.0676, \Omega_2 = 1.06$; (iv) GG strong: $\alpha_1 = 1, \alpha_2 = 1, \beta_1 = 4, \beta_2 = 1.71, \Omega_1 = 1, \Omega_2 = 1$; and (v) GG Moderate: $\alpha_1 = 1, \alpha_2 = 1, \beta_1 = 5.42, \beta_2 = 3.79, \Omega_1 = 1, \Omega_2 = 1$.

Fig. 2 shows the predicted and simulated OP performance versus the SNR for FSO, two values of pointing error parameter ξ and r of 1 and 2 with DGG moderate turbulence, m =1 and $\mathrm{SNR_{RF}}$ of 20 dB. for the Scenario I. As observed, there is a close match between predicted and Monte Carlo simulation results. We further consider $\phi_{1/2} = 60^0$, ψ=60^0. It is observed that, HD achieves lower outage compared with DD, which is as expected. For example, in the case of perfect

link alignment, to achieve an OP of 10^{-1}, the SNR of 9 and 11 dB are required for the HDand DD methods, respectively. This performance improvement is achieved at the cost of a more complex Rx. It can be also observed that, performance improves as the effect of the pointing error decreases. For example, for the DD method, to achieve an $\mathrm{OP} = 10^{-1}$, 20 dB is required for the perfect alignment case while this increases to 23 dB with of the pointing error.

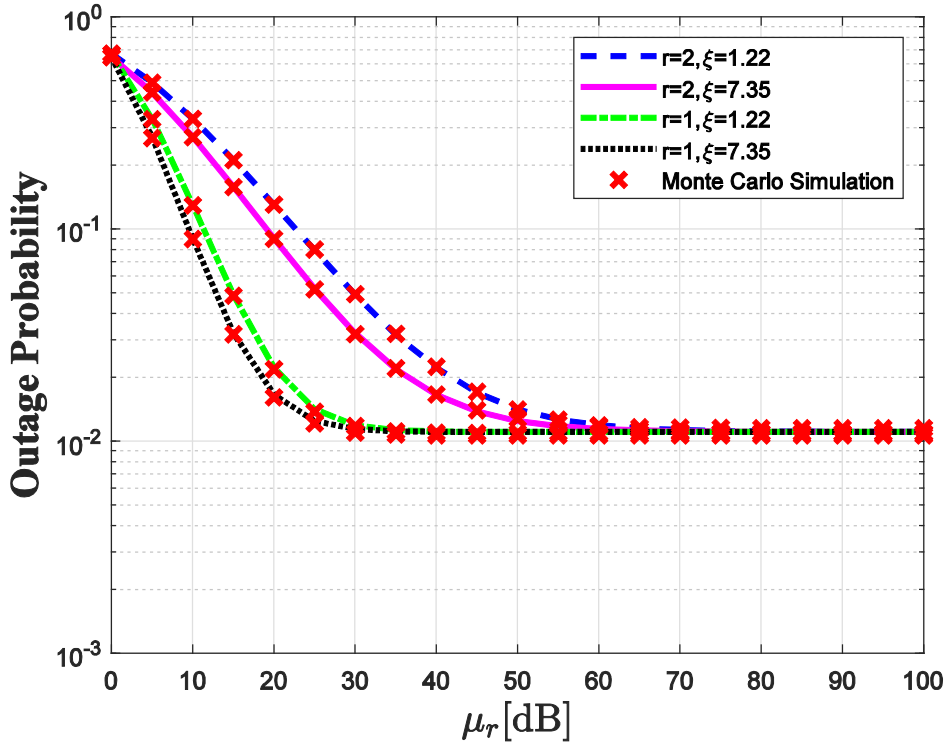

Figure 2: OP versus FSO SNR

Fig. 3 shows the predicted and simulated OP performance versus the semi-angle of VLC, for two values of ψ and L with DGG moderate turbulence, m =1, $\mathrm{SNR_{RF}}$ of 20 dB, $\xi = 7.35$ and $r = 1$ for the Scenario II. It can be seen that, OP improves with ψ. For example, for $L = 2\mathrm{m}$, to achieve an OP of 10^{-2},a semi-angle of 48° is required for $\psi = 80^{0}$, which increases to 51° for $\psi = 60^{0}$. It can be also deducted that, the OP performance improves as the height of the room decreases.

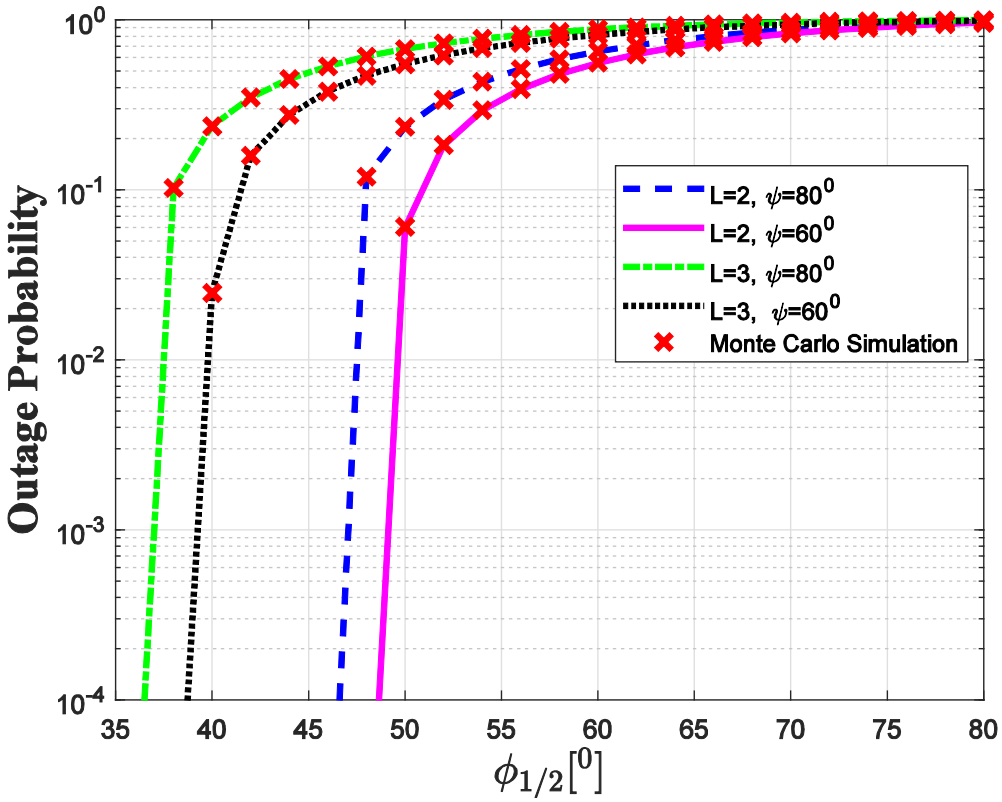

Figure 3: OP versus semi-angle of LED

Fig. 4 shows the predicted and simulated OP performance versus the SNR for FSO for $\alpha_1, \alpha_2, \beta_1, \beta_2, \Omega_1, \Omega_2$, m =1, SNR_{RF} of 20 dB, $\xi = 7.35$ and $r = 2$ for the Scenario III. As expected, from strong to the moderate atmospheric turbulence, the performance improves. Specifically, to achieve an OP=10^{-2}, SNR of 18, 29, 36 and 46 dB are required, respectively for DGG strong, DGG moderate, GG strong and GG moderate turbulence conditions.

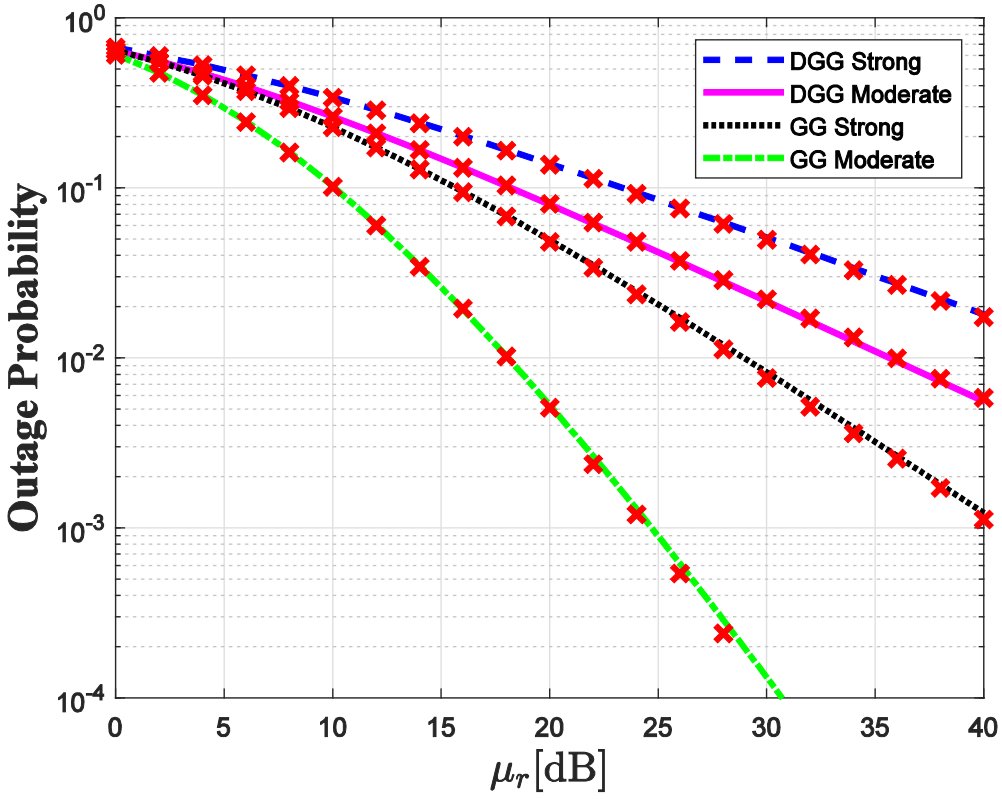

Figure 4: OP versus FSO SNR

Fig. 5 shows the predicted and simulated OP performance versus the SNR for RF, four values of RF severity parameter m and r of 1 with GG moderate turbulence, m =1, $\mu_r = 80$ dB, ψ=60^0 $\phi_{1/2} = 60^0$, and SNR_{RF} of 20 dB for the Scenario IV. As observed, the SNR values of 8, 11, 18 and 30 dB, respectively are required for $m = 1, 2, 4, 8$ for the outage of 0.001. As can be seen, by increasing m, the OP reduces systematically. In addition, it can be seen that, the relative distance between the curves reduces for higher values of m. This implies that its impact becomes increasingly less pronounced.

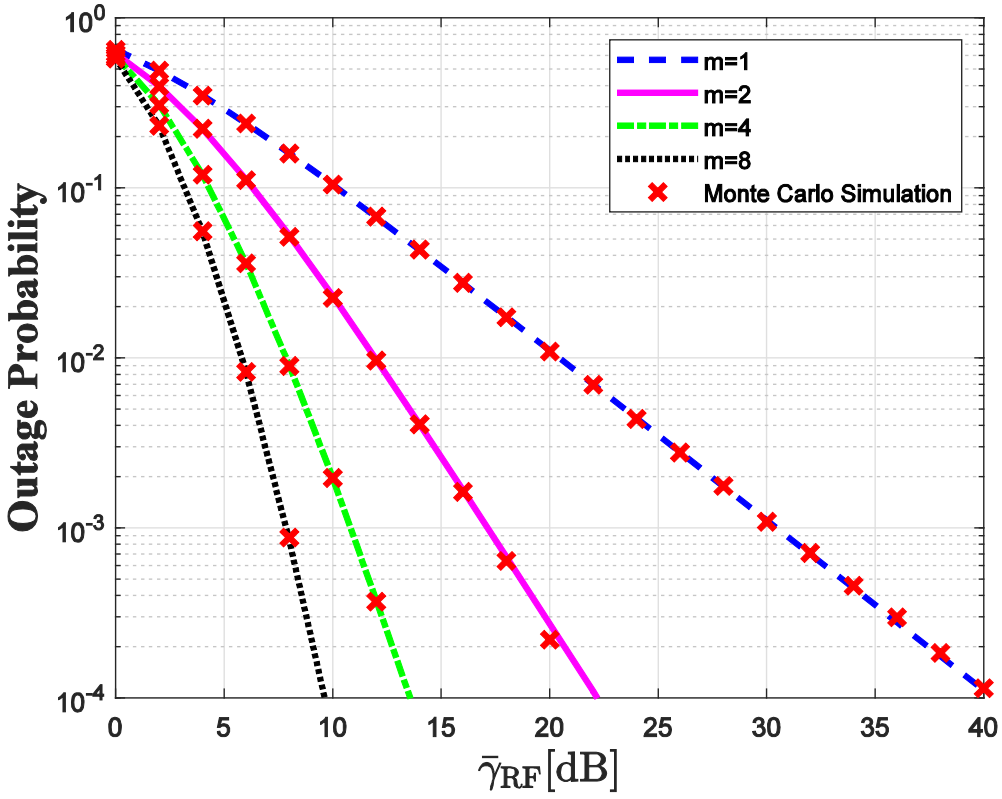

Figure 5: OP versus RF SNR

Finally, Fig. 6 shows the predicted and simulated OP performance versus power of VLC Tx, two values of semi-angle ϕ and N of 1 and 8 with DGG moderate turbulence, m =1, $r = 2$, $\mu_r = 80$ dB, $\bar{\gamma}_{\mathrm{RF}} = 20$ dB and $\mathrm{SNR}_{\mathrm{RF}}$ of 20 dB for the Scenario V. As expected, increasing the number of LEDs enhances the outage performance. For example, to achieve an OP of 10^{-2} we need 19 dBm transmission power of one LED, while this decreases to 15 dBm in the case of eight LEDs. Moreover, if we increase the semi-angle of the VLC link we need more transmit power of LEDs. For example, in the case of $N = 8$ and to achieve 0.01 of BEP, we need 3 dBm of transmission power for $\phi = 20^{0}$ while this increase to 15 dBm for $\phi = 80^{0}$. As observed, after a certain point, increasing the transmission power of LED has no effect on OP and a saturation takes place.

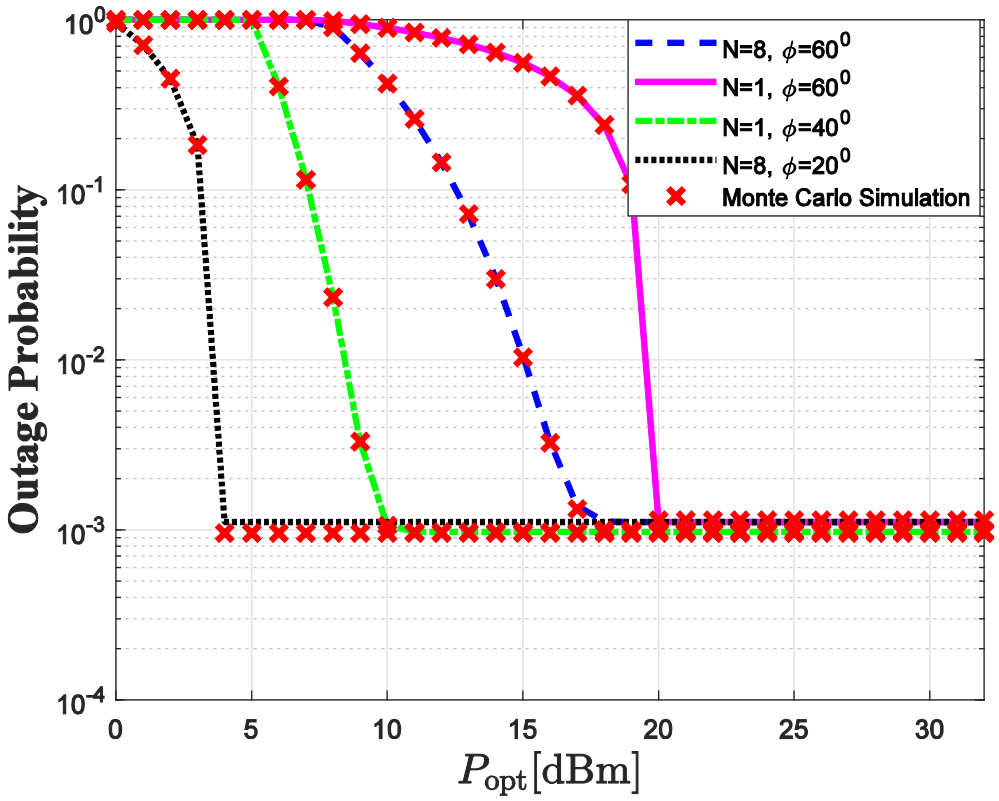

Figure 6: OP versus P_{opt}

5 Conclusion

We investigated the performance of dual-hop and triple-hop serial combinations of RF, FSO and VLC links. We assumed five different scenarios. We provided closed-from expressions for the OP and examined the accuracy and correctness of the derived expression by means of Monte Carlo Simulations. We showed that, increasing RF severity parameter, improvement of FSO turbulence conditions, increasing FSO pointing error parameter, decreasing the room height and increasing the number of LEDs resulted in improved outage and error performance.

References

[1] S. Arnon, J. R. Barry, G. K. Karagiannidis, R. Schober, and Eds M. Uysal. *Advanced Optical Wireless Communication Systems*. Cambridge, U.K. : Cambridge Univ. Press, 2012.

[2] Z. Ghassemlooy, W. Popoola, and S. Rajbhandari. *Optical Wireless Communications: System and Channel Modelling With MATLAB*. CRC Press, 2nd edition, 2019.

[3] M. Dohler and Y. Li. *Cooperative Communication: Hardware, Channel and PHY*. John Wiley & Sons, 2010.

[4] M. I. Petkovic, M. Narandzic, D. Vukobratovic, and A. Cvetkovic. Mixed RF-VLC relaying system with radio-access diversity. In *Proc. Wireless and Optical Commun. Conf. (WOCC)*, Beijing, China, May 2019.

[5] M. Petkovic, A. Cvetkovic, and M. Narandzic. Outage probability analysis of RF/FSO-VLC communication relaying system. In *Proc. Int. Symp. Commun. Systems, Netw. Digital Signal Process. (CSNDSP)*, Budapest, Hungary, July 2018.

[6] M. Namdar, A. Basgumus, T. Tsiftsis, and A. Altuncu. Outage and BER performances of indoor relay-assisted hybrid RF/VLC systems. *IET Commun.*., 12(17):2104–2109, Oct. 2018.

[7] A. Gupta, N. Sharma, P. Garg, and M. Alouini. Cascaded FSO-VLC communication system. *IEEE Wireless Commun. Lett.*, 6(6):810–813, Dec. 2017.

[8] C. Zhang, J. Ye, G. Pan, and Z. Ding. Cooperative hybrid VLC-RF systems with spatially random terminals. *IEEE Trans. Commun.*, 66(12):6396–6408, Dec. 2018.

[9] E. Soleimani-Nasab and M. Uysal. Generalized performance analysis of mixed RF/FSO cooperative systems. *IEEE Trans. Wireless Commun.*, 15(1):714–727, Jan. 2016.

[10] B. Ashrafzadeh, E. Soleimani-Nasab, M. Kamandar, and M. Uysal. A framework on the performance analysis of dual-hop mixed FSO-RF cooperative systems. *IEEE Trans. Commun.*, 67(7):4939–4954, July 2019.

[11] I. S. Gradshteyn and I. M. Ryzhik. *Table of Integrals, Series and Products*. Elsevier Inc., seventh edition, 2007.

[12] E. Soleimani-Nasab, M. Matthaiou, and G. K. Karagiannidis. Two-way interference-limited AF relaying with selection-combining. In *Proc. IEEE Int. Conf. on Acoustics, Speech and Signal Process.*, pages 4992–4996, Vancouver, Canada, May 2013.

[13] A. Mathai, R. K. Saxena, and H. J. Haubold. *The H-Function: Theory and Applications*. New York, NY, USA: Springer, 2010.

[14] Mohammadreza Kashani, Murat Uysal, and Mohsen Kavehrad. A novel statistical channel model for turbulence-induced fading in free-space optical systems. *J. Lightwave Technol.*, 33(11):2303–2312, June 2015.

[15] Wolfram. The Wolfram functions site. Available: http://functions.wolfram.com, 2020.